https://doi.org/10.1016/j.engstruct.2020.111799

The seismic behaviour of precast concrete interior joints with different connection methods in assembled monolithic subway station

Hongtao Liu [a,b], Zhenyu Wang [b], Xiuli Du [b,*], Geoffrey Q.P. Shen [c]

[a] *School of Civil and Transportation Engineering, Beijing University of Civil Engineering and Architecture, Beijing 100044, China*

[b] *Key Laboratory of Urban Security and Disaster Engineering of the Ministry of Education, Beijing University of Technology, Beijing 100124, China* [c] *Department of Building and Real Estate, Hong Kong Polytechnic University, Hong Kong 999077, China*

Abstract

The study investigated the performance of a specific full-scale precast concrete interior joint using many connected methods (e.g. grouted sleeves, anchorage arrangements, corbels) in the core region of joint, whilst a monolithic cast-in-place concrete specimen served as a control. The important indexes in terms of failure mode, hysteretic behavior, strength, deformation performance, and stiffness degradation were investigated under low- reversed cyclic loading. The new cross-lapping connection of concrete slab was presented and the position of the interface between two layers of lamination slab was optimized. The experimental and analysis results indicated that, (1) the precast concrete specimens were capable of matching peaking strength and deformation performance of the monolithic cast-in-place joint, while the displacement ductility and failure modes of two joints were different; (2) the elastic–plastic boundary of 1/550 which was used to evaluate precast structures should be carefully selected in the design; (3) an effective range for the thickness ratio of upper layer (post-pouring concrete) and lower layer (precast concrete) was presented; (4) a new cross-lapping connection for bend-up reinforcement at the ends of the semi-precast slab was performed for another optional method.

1. Introduction

The seismic and durability performance of structures could be obviously affected by the assembled and connected technology between precast elements. The concrete beam-slab-column interior joints composed of concrete beams, slabs and columns were subjected to combined effects of compression, bending and shearing forces in the case of seismic loads. The core region of joint withstands large internal forces to balance the external loads at the ends of the beam and column. Multiple earthquake damages indicate that structural collapses were caused by connection failure of joint without following the strong joint weak member concept. For the precast structure, each precast element was assembled and installed at the core region of joint, which increased the forcing complexity of joint.

The connected and assembled forms of precast structures including prestressed tendon connection [1–4], bolt connection [5–7], cast-in- place concrete connection(post-pouring) [8], grouted splice connection (grouted sleeves, metal bellows, constraint grout-filled lap connection) [9–11] have been extensively investigated and employed in a wide variety of structural application [12]. The prestressed tendon and bolt connections were grouped into dry-connector [13,14], which was convenient construction without post-pouring concrete on-site and exhibited excellent deformability. For example, the deformation behavior was primarily dominated by the opening of a gap that occurred at the interfaces of precast elements connected with prestressing tendons or bolts. However, the integrality and energy dissipation capacity of structures with dry-connector should be improved [15,16] by adopting proper structural solutions [17,18] including energy-consuming rebar and damping rubber. On the contrary, the cast-in-place concrete and grouted splice connections were labeled as wet-connector [19]. The cast-in-place concrete (post-pouring concrete), which was generally combined with grouted sleeves, was utilized to connect precast elements or composite members such as laminated

beam and slab. The specimens with wet-connectors exhibited excellent construction time and better quality control. It was noteworthy that the integrality was capable of matching the performance of the cast-in-place monolithic connections [20]. In particular, the grouted sleeves connection offered a popular option for many structures because of the insured better connection of discontinuous bars and related ease of construction.

The assembled monolithic concrete structure was a new type of structural system combined cast-in-place structure and precast structure connected by grouted sleeves which have been therefore recommended for the applications in the underground station [21], as shown in Fig. 1. The bottom slab of station was poured in on-site concrete. After precast sidewalls and columns were placed in their designed positions and connected with grouted sleeves, then a flowable grout injection in each gap which played an important role in transferring stress. Finally, the on-site concrete was utilized to improve the structural integrity after semi-beam and semi-slab were assembled and installed. The mechanical behavior was complicated in the core region of joint due to the dense arrangement of steels and complicated connection methods.

The seismic behavior of the joint relies largely on the connection between precast elements, and to some extent was affected by the laminated slab. The thickness of the laminated slab used in underground structures was larger than that of the above-ground structure (about 120 mm). When the cast-in-place layer thickness was greater than 60 mm, the laminated slab could be considered as cast-in-place slab based on the plane section assumption and enough bonded strength at the interface between cast-in-place concrete and precast concrete in the laminated slab [22]. Increasing the shear keys in the one-way or two- way laminated slab to improve the bonding strength was an effective measure [23,24], but it has limited effects on the yielding strength and deformation. Li et al. [25,26] proposed a new laminated pouring technique for the composite slabs, and investigated the influence of bonding strength on the structural behavior. Experimental results showed that the failure mode of the laminated slab was primarily dominated by the longitudinal shear bond strength regardless of

lamination thicknesses. Therefore, the thickness of post-pouring and precast layer in laminated slabs could be optimized to decrease the interface stress.

In light of the above-mentioned background, this paper aims at investigating the seismic performance of precast beam-slab-column interior joint based on the cross-section of the assembled monolithic concrete subway station. Although the seismic behavior of underground subway station was safer than aboveground structures, the collapse failure of Daikai station has received significant attention in recent decades [27]. Furthermore, the seismic performance of transverse direction should be received significant attention, as shown in Fig. 1 [21]. Therefore, the present work was organized as followed, the detailed experimental program of the precast beam-slab-column joint was presented. Meanwhile, a monolithic cast-in-place concrete specimen with identical details served as a control. Then the seismic behavior of the specimens was investigated in terms of failure mode, hysteretic behavior, stiffness degradation, strain distribution, energy dissipation and deformation. Finally, the recommended range for each layer thickness was introduced for laminated slabs in which arrangement could avoid bond splitting cracks. The research outcome of this study will provide an in-depth understanding of the inherent mechanisms of precast joint and lay a foundation for further application of assembly technology.

2. Experimental program

2.1. *Specimens design*

Two full-scale beam-slab-column interior joints including cast-in- place interior joint (CIJ) and precast interior joint (PIJ) are constructed and experimentally tested under a constant axial load and a cyclically reversed load. Specimens are taken out from the two-story three-span subway station, as shown in Fig. 1. Combined with the loading equipment of 40000KN capacity multifunctional electrohydraulic servo loading system, the construction dimensions of specimens with approximately 5000 mm in height and 6300 mm in length are determined based on the overall bending moment

diagram of subway station. The width of specimen is 2400 mm because of the limited space of the loading equipment. The column has a height of 5000 mm and a rectangular cross-section with 700 mm × 900 mm, and the cross-section of beam member is 1000 mm × 1000 mm.

The precast specimen is composed of two precast column elements, two semi-precast beam elements and four semi-precast slab elements. The twenty-four pieces of 28 mm diameter HRB400 (24C28) longitudinal reinforcement are distributed around the cross-section of column, which has an approximate longitudinal reinforcement ratio of 2.34%, as shown in Fig. 2 and Table 1. Additionally, the transverse reinforcement ratio of 1.25% is provided with 12 mm diameter HRB400 triple hoops deformed bars at 100 mm spacing along the height of column. The configuration of longitudinal reinforcement and transverse reinforcement meets the requirements of the code [28,29]. The semi-precast beam is divided into two parts (left and right beams) and the distribution details of steels are shown in Fig. 3. The reinforcement ratio of the longitudinal reinforcement of slabs is 1.42%, and the reinforcement ratio of the distribution bars and stirrups is 1.13%, as indicated in Fig. 4. In order to improve sufficient adhesion strength between post-pouring concrete and precast concrete, the precast slab surface is roughened.

For different precast parts, the connection types of steels are different. Fig. 2 shows that the longitudinal bars in the precast column are connected using commercially available grouted sleeves. The manner of straight splicing is utilized to connect the precast beam elements, as shown in Fig. 3. Mostly, the overlapping length of the precast beam bars is 900 mm, which is about 32 times diameters of longitudinal steel and meets the overlapping requirements [29]. According to the code for the design of concrete structures [29], the concrete laminated slab with hanger bars should be considered and adopted when the span of concrete slab is greater than 3 m. The total thickness of the concrete slab is 400 mm, in which the cast-in-place layer and the precast layer are 200 mm, respectively. The bars of laminated slab are arranged with double-deck bars, and the upper and lower bars are connected by hanger

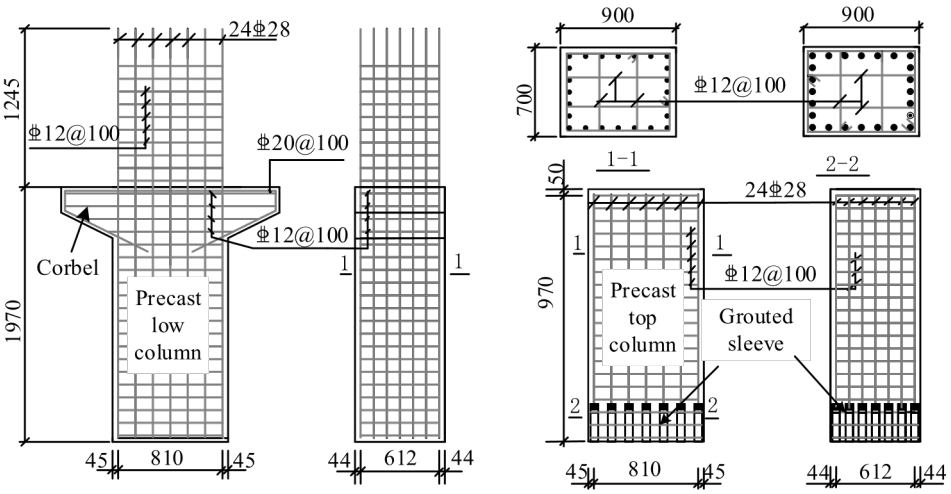

Fig. 2. Precast column details.

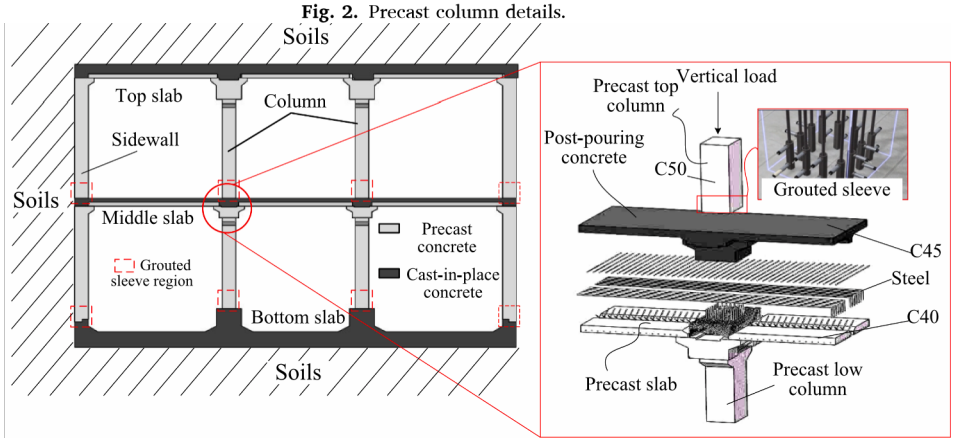

Fig. 1. Cross-sectional plan of assembled monolithic concrete structure [21].

Table 1

Parameters of specimens.

Specimens	Element	Section size/mm	length/ mm	Longitudinal reinforcement	Longitudinal reinforcement Ratio/%	Transverse reinforcement	Ratio of transverse reinforcement/%	Axial compression ratio
PIJ	Precast column	700 × 900	2000	24C28	2.34	4C12@100	1.25	0.85
	Precast beam	1000 × 600	2600	20C25 (2C22)	1.76	6A10@100	1.23	——
	Precast slab	1100 × 200	2650	C22@150	1.42	A10@300 × 600 C18@150	1.13	——
CIJ	Column part	700 × 900	5000	24C28	2.34	4C12@100	1.25	0.85
	Beam part	1000 × 600	2400	20C25 (2C22)	1.76	6A10@100	1.09	——
	Slab part	2400 × 400	6300	C22@150	1.42	A10@300 × 600 C18@150	1.13	——

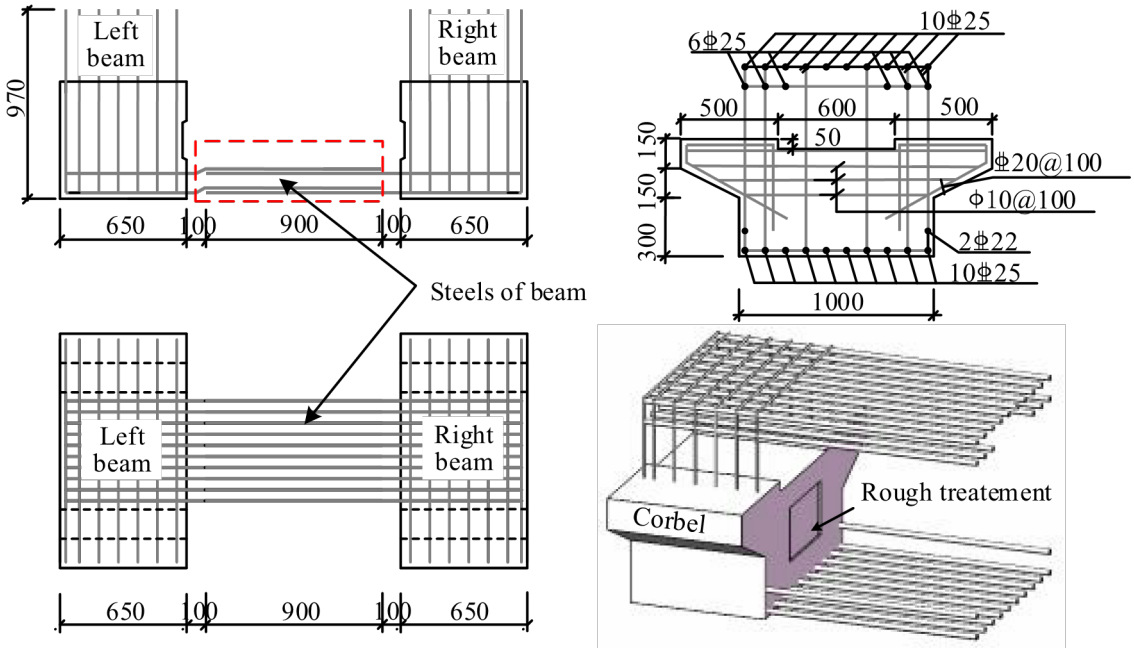

Fig. 3. Precast beam details.

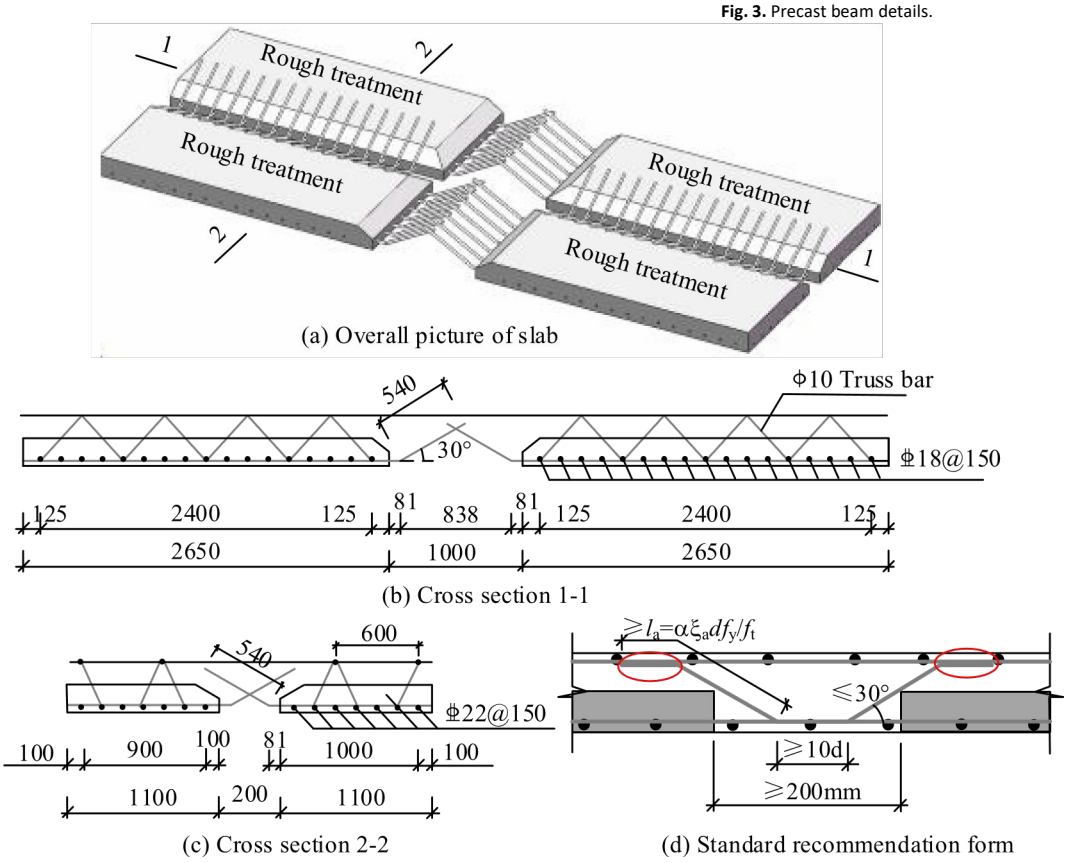

Fig. 4. Laminated slab details.

bars, which provides the integrity of the steel cage and improves the bonding strength of the interface between precast and cast-in-place concrete. Meanwhile, the spacing of hanger bars should not be

greater than 600 mm, and the width of the post-pouring region should not be less than 200 mm based on the Chinese code [22], and the cross-lapping connection is adopted according to the bend-up reinforcement at the ends of semi-precast slabs (shown in Fig. 4(a)). It is noteworthy that the arrangement of bend-up reinforcement in the post-pouring region is different from the standard recommended form, as shown in Fig. 4(d). Bending the steel before the steel bar contacts to avoid the over-dense and overlapping of bent-up reinforcement is an effective measure, as shown in Fig. 4.

A monolithic cast-in-place concrete specimen with identical details including cross-section, reinforcement ratio and concrete strength, etc. is served as a control, as shown in Fig. 5. Only difference between the precast concrete and cast-in-place concrete is the different connection types of concrete elements. For example, the continuous steels are used to replace grouted splices, lapping connection and cross-connections for cast-in-place column, beam and slab, respectively. In addition, the grouted splices can lead to decreasing of concrete cover (16 mm instead of 30 mm). In spite of this, the concrete cover of cast-in-place part is formed as much as the precast part.

The main steps and key points of the assembly process are as follows. The precast members are cast and processed in the prefabricated element factory, and they are assembled and installed on-site. The semi- precast beam is connected to the precast column with corbel, and the semi-precast slab elements are placed on the edges of the semi-precast beam, followed by continuous steel which is placed at the top surfaces of the precast slabs and beams. Meanwhile, the continuous steels and post-casting concrete

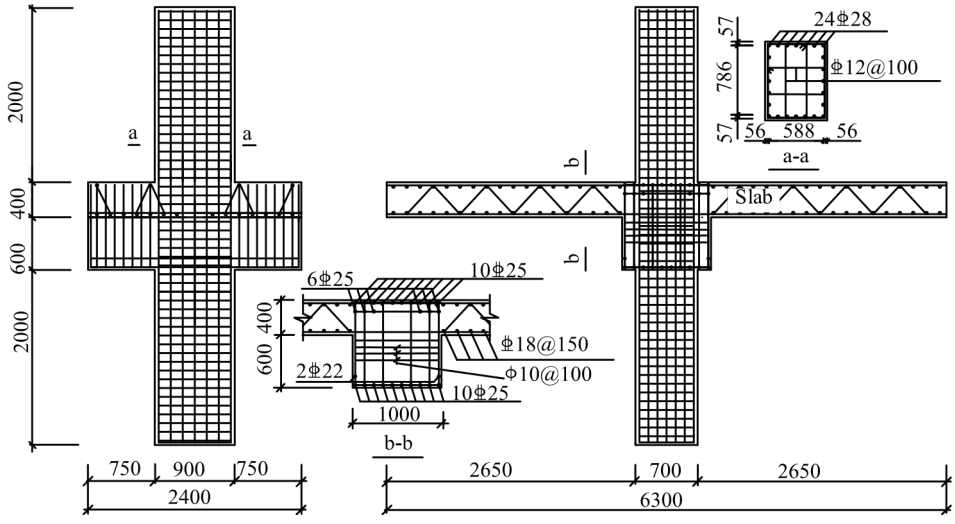

Fig. 5. Cast-in-place specimens details.

are utilized to connect all semi-precast members and form an emulating monolithic reinforced concrete joint. Finally, the upper precast column is connected by the grouted sleeves. It is noteworthy that the contacting surface of the semi-precast element is roughened to transfer the shearing force and increase adhesion to the surrounding cast-in-place element, which has been reported by Wang [30]. Each part

and construction process of precast specimen is depicted in Fig. 6. The cast-in-place specimen is constructed using traditional construction methods. That is to say, the reinforcing cage fabrication and concrete casting of CIJ specimen are completed by one time, as shown in Fig. 7.

2.2. *Materials*

The concrete grade of the precast column and other semi-precast elements are C50 and C40, respectively. It is noteworthy that the post- pouring concrete grade is C45 [22], and the purpose is to improve the bond strength between precast and cast-in-place concrete. The relevant material parameters of concrete, reinforcement bars and grouted sleeves are presented in Table 2. More details about the cementitious grout for splices are available in Ref. [31]

2.3. *Test setup*

The loading setup and protocol are shown in Fig. 8(a). The ends of specimen can be regarded as the point of contra-flexure and the bending moment values are equal to zero, which could meet the real force state of the joint in the overall structures. The top and bottom of the specimen are fixed by two spherical hinges, and the constant vertical load of 12260kN (corresponding to the axial compression ratio of 0.85) is applied to spherical hinge support, which is consistent with the vertical load subjected to column [33]. The other two actuators are installed at both ends of slabs through the reserved holes and applied equal but reverse forces that stand for deformation of slab under seismic loads. The cyclic loading with loading ratio of 0.1%Hz is generally load-controlled up to yield load at first and displacement-controlled up to failure with increasing displacement ductility coefficient [34], and the cyclic loading protocol adopted in the test is presented in Fig. 8(b). It is planned to remove the applied load on the load-end when the strength decreases to 85% of the maximum achieved strength.

The response quantities of interest include cracking distribution, bending deformation, strength, cracking width and overall deformation. Fig. 9 shows the distribution of the dial indicators (DI) and linear variable deformation transducers (LVDT). Two dial indicators (C1, C2) are installed at bottom of the precast low column to measure the bending deformation, and two dial indicators (X1, X2) are used to measure the cracking width of the interface between the semi-precast slab and post- pouring concrete. The overall deformation of slabs is expressed by six linear variable deformation transducers (L1, L2, L3, L4, L5, L6). Additionally, the distance between the measuring points of the overall deformation is 800 mm.

3. Test results

3.1. *Slab crack distribution analysis*

All specimens underwent the typical flexural dominated response damage controlled by the developing of plastic hinges at the slab and experienced four major damage states (cracking, yielding, peaking and failure). Due to the different construction methods of cast-in-place and precast specimens, the failure modes of both specimens were different. The specific failure process of specimens was as follows.

The cast-in-place specimen was tested as a reference specimen. The first horizontal crack was noticed at the bottom of slab when the strength was 120kN, as shown in Fig. 10(a). The cracks were mainly located at the bottom of the slab and concentrated within one-half slab thickness from the end of slab as expected. The horizontal cracks continued to propagate along the length of the slab with increasing levels of imposed vertical displacements. When the strength of the specimen was about 300kN, cracks have extended to 2.5 times thicknesses of the slab from the slab-end. The slightly inclined flexural- shearing cracks with the length of 200 mm occurred at the interface between beam

part and slab part. Although cracks did not link up, the specimen has almost reached its yield strength at a displacement of 22 mm (yield displacement), as shown in Fig. 10(b). When the specimen was subjected to 5 times yielding displacements, well-distributed flexural cracks formed and appeared at the top and bottom of slab, which mainly located within half-thickness of slab from the slab-end. It was observed that the concrete in the vicinity of the interface between slab and beam was damaged seriously. Meanwhile, the specimen reached its peaking strength. When the specimen was subjected to 10 times yielding displacements, the plastic hinges adjacent to the beam were formed, and failure was characterized by crushing and spalling of the concrete. On the contrary, there was no evident damage in the column. The map of the cracks of failure mode was shown in Fig. 10(c).

The failure progress of specimen PIJ during the cyclic tests was identical to the respective failure modes observed in the specimen CIJ tests. It can be observed that prior to yielding the specimen was in the elastic state and the deformation could be recovered by itself. The first crack occurred when specimen PIJ was subjected to 159kN which was roughly 32.5% more than that of the cast-in-place specimen. It indicated that the cracking strength of PIJ was comparable to (even superior than) the conventional cast-in-place connections. It should be noted that the first visible crack was in the interface region between the semi-precast slab and post-pouring concrete, as shown in Fig. 11(a). As observed, the crack of laminated slabs extended along the length of the specimen with the increment of the deformation of slab-ends. The specimen

Fig. 6. Construction process of precast specimen PIJ.

Fig. 7. Construction process of cast-in-place specimen CIJ.

Table 2
Mechanical properties of materials.

Materials	Grade	d/mm	f_y/MPa	f_u/MPa	E_s/MPa
Reinforcement	HRB400	28	420.6	593.9	2.1×10^5
		25	454.4	617.0	2.1×10^5
		22	446.5	574.9	2.1×10^5
		18	436.2	564.1	2.0×10^5
	HPB300	10	309.3	451.3	2.2×10^5
Grouted sleeve [32]	GT-28	Carbon steel	387.0	663.0	$2.05 \times 10_5$
Concrete	Strength	f_{cu}/MPa	f_c/MPa	E_c/MPa	υ
	C40	45.4	26.6	$3.14 \times 10_4$	0.2
	C45	51.1	29.3	$3.38 \times 10_4$	0.2
	C50	55.9	32.7	$3.33 \times 10_4$	0.2

Note: d is diameter of steel; f_y is yielding strength of steel; f_u is ultimate strength of steel; E_s, E_c are elastic modulus of steel and concrete, respectively; f_{cu} is compressive strength of concrete cube; f_c is the compressive strength of concrete prism; υ is Poisson's ratio.

achieved the yielding strength of 290kN at a displacement of 13.58 mm. Two main penetrated cracks of slab concentrated in the region of 500 mm away from the beam corbel. Moreover, the obvious bond splitting cracks were observed between precast semi-precast slab and corbel of precast beam. Besides, the visible vertical cracks appeared on the sides of the specimen, and mainly distributed in the range of 300–500 mm from the beam corbel. The crack distribution corresponding to the yielding state was recorded in Fig. 11(b).

After the specimen yielded in succession, cracks began to spread rapidly along the length of slabs. Meanwhile, the drawbacks of the precast specimen were exposed. For example, more localized cracks

and gaps were observed at the interfaces between precast elements and post- pouring elements (such as semi-precast slab and precast beam, semi- precast slab and post-pouring concrete). The opening and subsequent closing of gaps occurred because there were no effective strengthening measures. Additionally, inclined cracks of laminated slabs were located at the top of the beam corbel. The peaking strength of the specimen was obtained when the displacement of slabs reached 5 times yielding

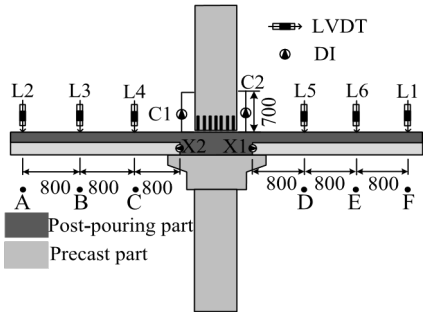

Fig. 9. Installation position of instrumentation.

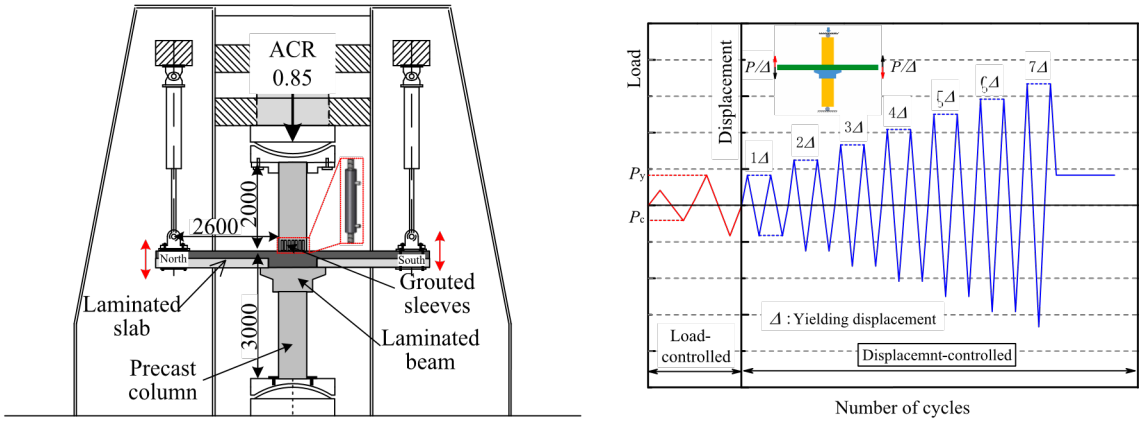

(a) Loading setup (b) Loading proctocol

Fig. 8. Loading setup and protocol.

Fig. 10. Failure process of CIJ.

displacements. With the increment of displacement, the debonding splitting failure of laminated slabs occurred in the interface of precast and post-pouring elements, which was the noticeable difference with the cast-in-place specimen. The debonding splitting failure length of the laminated slab was 2 times thicknesses of slabs and the maximum size of cracks increased to 5 mm. The failure state of the precast specimen was shown in Fig. 11(c).

Compared with the cast-in-place specimen, the following observation was realized. Although the crack propagation process of the precast specimen during the cyclic tests was identical to the respective process observed in the cast-in-place specimen, the failure modes of both were different. The failure patterns were mainly reflected in the following two aspects. Firstly, the bond strength of the interface

between semi-precast slab and post-pour concrete was weak, which seems to be the main reason for the splitting failure of laminated slabs. Secondly, the corbels of the semi-precast beam lead to redistribution of internal force in the laminated slab. The distribution of plastic hinges was different obviously. For example, the plastic failure region of CIJ was distributed within 600 mm from the beam, while the plastic region of precast specimen extends outward, approximately within the range of 800 mm outside the corbel of semi-precast beam. Meanwhile, the specimen PIJ exhibited a significant deformation caused by bond-slip at the contact surface between precast slab and semi-precast beam. On the while, the main damages were mainly concentrated in the plastic hinge region of slab, which was in line with the strong-joint-weak-member concept in the seismic resistant design.

3.2. *Loading-displacement hysteretic response and backbone curves*

The recorded relationship curves of force and displacement were plotted in Fig. 12. According to the loading setup and protocol, as shown in Fig. 8(a). The horizontal axis represents the vertical loading displacement at the slab-end, and the vertical axis corresponds to the force of the slab-end. On the basis of the hysteretic response, the following observation can be inferred:

(1) The significant pinching was observed in all specimens, and the inconspicuous asymmetric response of hysteretic curves was due to mainly dead weight of slab and construction tolerances, which was also found in previous concrete column experiments [35].

(2) In terms of deformation, it can be observed that prior to yielding of the specimen, the deflection of specimens could be self- recovery. However, when the specimen yielded in succession, the specimens gradually underwent plastic deformation and their stiffness gradually decreased.

(3) One noticeable difference between both specimens was that the peaking strength of the precast specimen was higher than that of the cast-in-place specimen. The main reason for the increase in the peaking strength was related to the position change of the plastic hinge of the laminated slab.

The positive and negative envelopes were combined to produce backbone curves, as shown in Fig. 13, which could reflect the deformation capacity and ultimate strength of specimens at different forcing stages. The displacement and strength at major damage state, such as

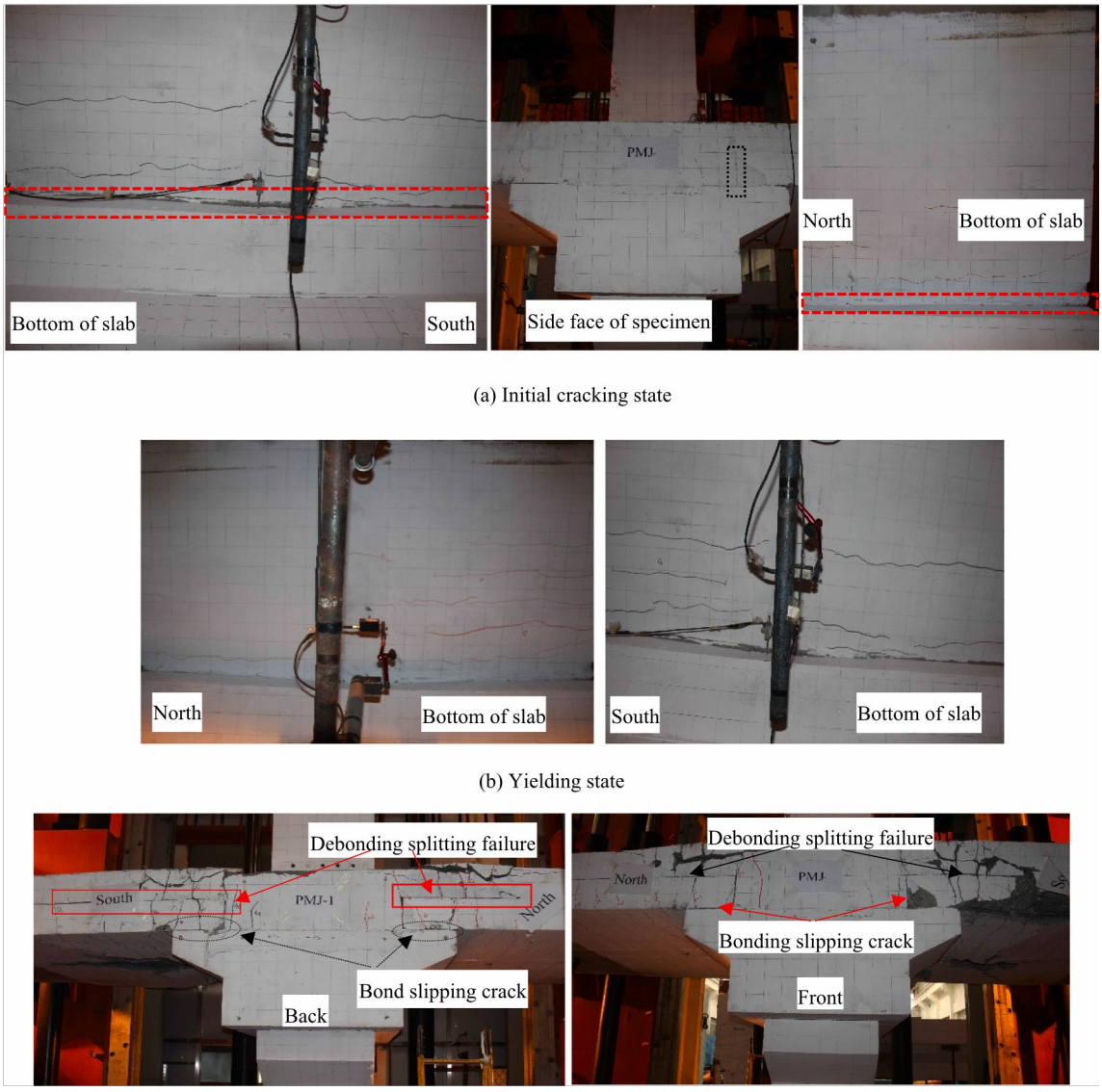

Fig. 11. Failure process and distribution of cracks of PIJ.

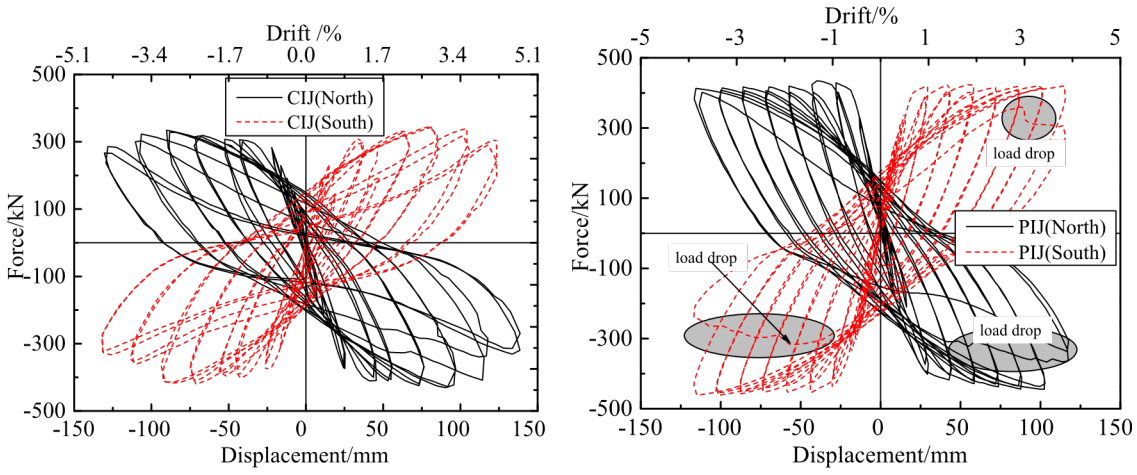

Fig. 12. Hysteretic curves of the testing specimens.

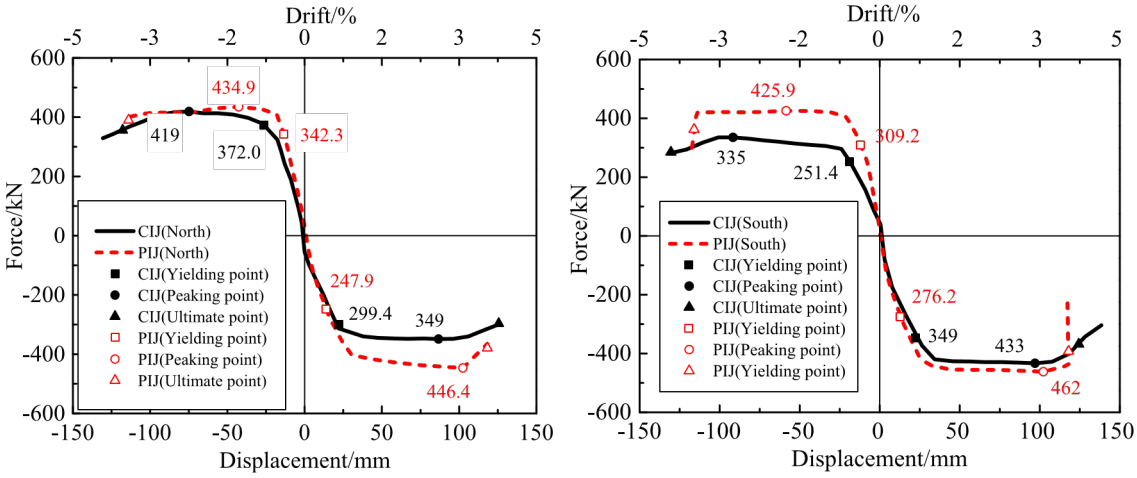

Fig. 13. Backbone curves of specimens.

Table 3
Feature point values of test results.

Specimens	Position	Loading direction	F_y/kN	Δ_y/mm	F_p/kN	Δ_p/mm	F_u/kN	Δ_u/mm	μ
CIJ	North	Positive	− 299.40	22.08	− 349.00	86.68	− 296.65	125.63	5.69
		Negative	371.97	− 26.51	419.00	− 74.83	356.15	− 117.83	4.44
	South	Positive	− 348.11	22.63	− 433.00	97.02	− 368.05	124.383	5.50
		Negative	251.38	− 18.67	335.00	− 91.66	284.75	− 130.47	7.00
PIJ	North	Positive	− 247.89	13.76	− 446.40	102.40	− 379.44	118.28	8.60
		Negative	342.28	− 13.41	434.90	− 42.64	369.67	− 124.90	9.31
	South	Positive	− 276.23	12.91	− 462.00	102.20	− 392.70	118.00	9.14
		Negative	309.19	− 11.88	425.90	− 58.46	362.02	− 116.00	9.76

yielding state, peaking state and ultimate state, were recorded and summarized in Table 3. The equivalent bending moment method was used to determine the yield state. More details on the definition method of each major damage loading point were given in Ref.[21]. $\Delta_{y,}\Delta_{p,}\Delta_{u}$ present the yielding displacement, peaking displacement and ultimate displacement, respectively; F_{y}, F_{p}, F_{u} stand for the yielding strength, peaking strength and ultimate strength, respectively; μ was displacement ductility which was obtained as the ratio of ultimate displacement $\Delta_u$to yielding displacement Δ_y of specimen; The positive was associated with the compression direction of the bottom of slab and negative with tensile.

From Fig. 13 and Table 3, one can see that all tested specimens achieved ultimate displacement which was significantly higher than the yielding displacement. It would seem to indicate that all specimens underwent ductile failure and had stable and excellent nonlinear responses [36].

(1) It should be noted that the obviously asymmetric response of backbone curves for the cast-in-place specimen under the low- cycle repeated load, especially for the peaking strength. Compared to the peaking strength of the cast-in-place specimen in the positive loading direction, the reduction in the strength was 19.7% for the negative loading direction. Otherwise, the maximum error was about 5.16% for the precast specimen, which was considered acceptable in view of many uncertainties in construction and assembly of the precast elements.

(2) Another issue to be commended was that yielding displacement of cast-in-place specimen was 1.73 times more than that of precast specimens, which was disadvantageous to deformation of precast structures subjected to the seismic loading. If the elastic–plastic limit of 1/550 of above-structures was adopted [37], the cast-in-place concrete structure was unsafe and should be reduced for the precast specimen.

(3) In terms of displacement ductility, the cast-in-place specimen attained displacement ductility level of about 5.66, while the ductility of precast specimen was 9.20. The main reason for larger ductility was that the opening gap contributed to the global deformation in the later loading. The comparative analyses of both specimens were described in Section 4.4.

3.3. *Stiffness degradation*

The stiffness degradation could reflect the damage level of the concrete. The secant stiffness (peak-to-peak stiffness) was defined as the slope of a line connecting the peaking loading points in the direction of positive and negative loading for a given cycle [36,38]. Fig. 14 showed that the stiffness degradation of each system varies at different drift levels.

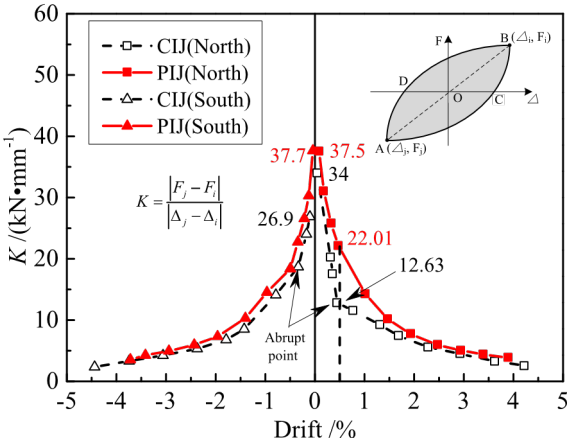

Fig. 14. Comparison of secant stiffness degradation curves.

In general, the secant stiffness decreased monotonously with increment of the drift level. The secant stiffness of the precast specimen was about 1.23 times higher than that of the cast-in-place specimen at the small drift with an elastic response. The determining method of yielding strength shows that the larger the secant stiffness was, the lower the yielding displacement of the precast specimens was. As the drift progressively increases up to 0.5%, the stiffness degradation of cast-in-place specimen

was faster than that of precast specimen. Furthermore, a stiffness abrupt was observed at a drift of 0.5% which was less than the yielding displacement of cast-in-place specimen. However, the stiffness degradation of precast specimen gradually declined. Beyond the drift of 0.5%, the precast specimen end up with the same secant stiffness as that of the cast-in-place specimen. Overall, the precast specimen delivered stiffness degradation similar to the conventional cast-in-place specimen. But the precast specimen seems to improve the initial stiffness of the system, which was mainly related to the assembled elements, connection type and grouted splices.

The stiffness degradations obtained from the hysteretic curve could reflect the deformation capacity, especially the concrete nonlinear deformation. The relationship between stiffness degradation and displacement ductility was investigated by Gulkan [39], as shown in Eq (1). Mohamed et al. [36] studied the response of the rectangular columns in terms of secant stiffness to displacement ductility when the parameters, α, was 1, and showed that the proposed formula conservatively predicted the stiffness degradation up to displacement ductility of 6. The normalized stiffness was defined as the ratio of secant stiffness, K, to yielding stiffness, K_y. Fig. 15 indicated the comparison of experimental results and the proposed equation obtained from Mohamed [36]. One can see that the proposed equation underestimated the stiffness degradation, so the parameter, α, was modified as 0.8, which agreed well with the experimental results. The correction curve was presented and plotted in Fig. 15.

$K1\_{y} = \mu_{a} \geqslant 1$ (1)

K

3.4. *Energy dissipation*

The energy dissipation capacity was an important index for evaluating the seismic performance of structures. Fig. 16 showed the energy dissipation coefficient h_e at each drift ratio which was calculated by Eq. (2). It should be noted that the area was obtained by the numerical integration of the force–displacement loop during the first cycle at each drift ratio when the specimen yielded in succession.

$$he = (SDBC + SDAC)/(SBOE + SFOA) \qquad (2)$$

As observed, the energy dissipation coefficient increased with an increase in the drift up to failure for all specimens. The main reason for

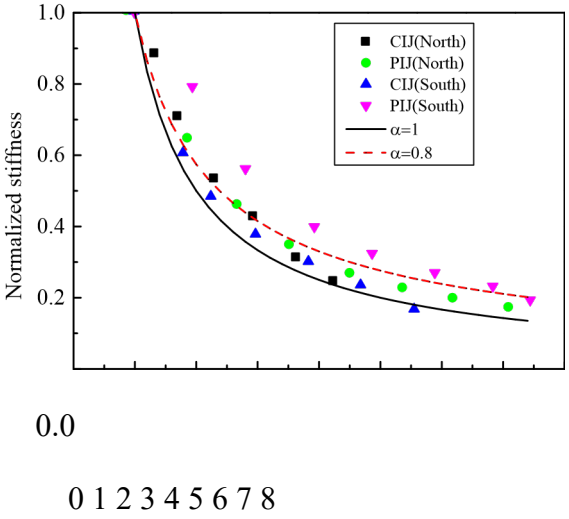

Fig. 15. Experimental versus analytical stiffness degradations.

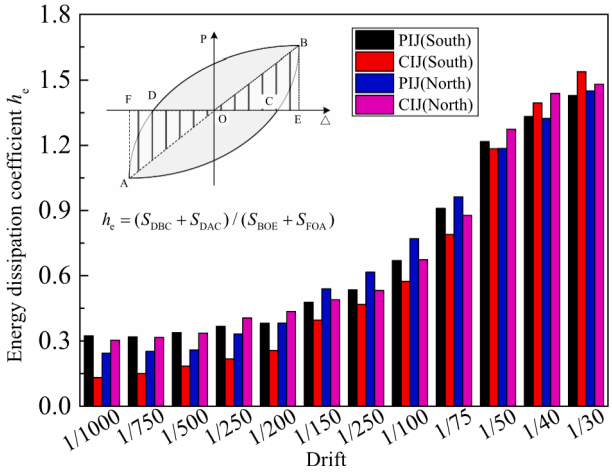

Fig. 16. Relationship curves between energy dissipation coefficient and displacement angle.

the above observation was that concrete damage gradually increased. When the drift was less than 1/500, the energy dissipation coefficient of specimen PIJ was slightly larger than that of the cast-in-place specimen. With the increment of drift, the energy dissipation coefficient has a linear relationship, which indicates that the damage of the specimen was developing uniformly. When the drift was greater than approximately 1/ 500, the energy dissipation capacity of the precast specimen was lower than that of cast-in-place specimens. On the whole, based on the test results, as long as precast elements were well designed and constructed, the energy dissipation of precast specimen was comparable with (and, in some case, even superior than) that of cast-in-place specimen.

4. Deformation analysis

Sufficient deformation capacity was the key to improve the seismic resistance of structures (especially underground structures). The deformation capacity of specimens was evaluated on the basis of strain change of grouted sleeves, bending deformation of columns, deformation distribution of slabs and the cracking width of interfaces between precast part and post-pouring concrete.

4.1. *Strain of grouted sleeve*

The grouted sleeves play a crucial role in connecting precast elements and transferring force through discontinuous bars [40]. However, the performance of grouted sleeves on the plastic hinge region was prohibited by most design codes [28]. Therefore, there was a need to

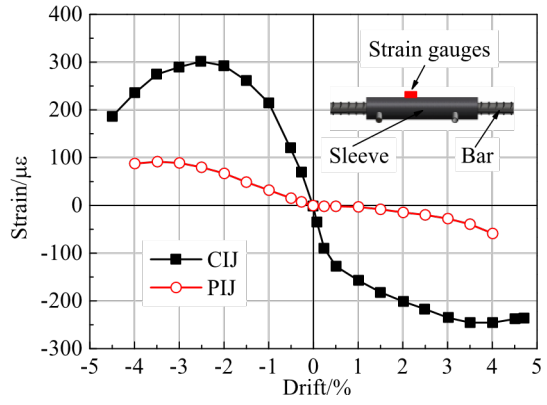

Fig. 17. Relationship curves between sleeve strain and deformation of loading end.

check and determine whether the grouted sleeve was yielding during the deformation process. Fig. 17 showed the axial strain of sleeve at different drift levels, and the contradistinctive steel strain of cast-in- place specimen was also plotted.

The strain of grouted sleeves was generally smaller than that of steel bars in the same position of specimen. Moreover, the strain was approximately proportional to drift, which indicated that grouted sleeves were in elastic phase and provided simplify treatment for calculating grouted splice in the numerical models. The maximum axial strain of the grouted sleeve was 100με and far less than the tensile strain of concrete, which indicated that the softening effect of bond-slip between grouted sleeve and concrete was not considered. It was worth mentioning that the steel strain in the cast-in-place specimen decreased after 2.5% drift that was basically corresponding to the peaking strength.

4.2. *Bending deformation of column*

The bending deformation was achieved as dominant component in the total deformation of the column, and it can be evaluated by bending angle, θ, which was obtained by dividing the deformation difference, C_1- C_2, with specified width of column section, L. Because the column corbels restrain the deformation of the precast low column, the bending deformation of the precast top column was only compared to illustrate the effect of grouted sleeve on the bending deformation. Fig. 18 showed the backbone relationship curves between bending angle and drift of loading slab-end. One can see that the bending deformation of the cast- in-place top column was much larger than that of the precast top column. Grouted sleeves in the precast top column improved the cross- stiffness and reduced the bending deformation. For example, the max bending angle of specimen CIJ was 0.889% at drift 1%, which was approximately 26.9 times more than that of the precast specimen.

4.3. *Overall deformation distribution of slab*

The vertical deformations of every measuring point A, B, C, D, E, F (illustrated in Fig. 9) were recorded during the test. Meanwhile, the overall deformations of specimens in the yielding strength state (F_y) and ultimate strength state (F_u) were plotted in Fig. 19.

On the whole, the overall deformation at the ultimate strength state was larger than that of yielding strength state, which showed that the plasticity of the specimen has been fully developed after it yielded in succession. The curves of A-C and D-F were approximately linear, which indicated that the plastic hinge region was mainly distributed in the C-D regions of 1300 mm distance from the specimen center. However, there was a noticeable difference in the deformation between both specimens. The vertical deformation of precast specimen at the yielding state was generally smaller than that of cast-in-place specimen. On the contrary,

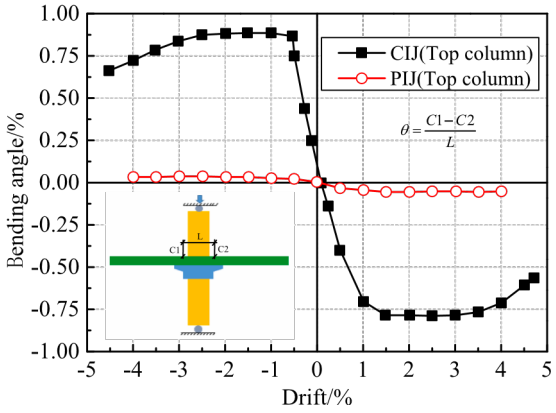

Fig. 18. Relationship curves between bending angle and drift at loading end.

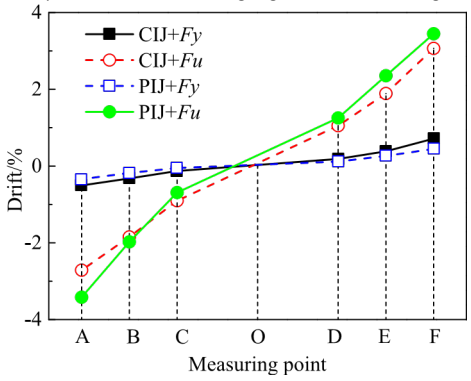

Fig. 19. Overall deformation distribution.

the deformation of precast specimen was larger than that of cast-in-place specimen at the ultimate state. As mentioned in Section 3.2, it was unreasonable and unsafe to utilize the limited yielding drift from the specification of cast-in-place structures to evaluate guidelines of precast structures. *4.4. Cracking width analysis*

Compared with the cast-in-place specimen, the integrality of the precast structure relies largely on the connecting strength between the precast element and precast element or post-pouring concrete, which was considered as the weak part and formed easily plastic hinge zone [41]. So the gaps between semi-slab and post-pouring of semi-beam were measured using dial indicators X1 and X2, as shown in Fig. 9. Simultaneously, the cracking width of the cast-in-place specimen with identical positions served as a control. One can see from Fig. 20 that the cracking width of precast specimen was much larger than that of cast-in- place specimen. Especially the drift was more than 1/100, the cracking width

of precast specimen propagated rapidly. The maximum cracking width of cast-in-place specimen was about 2.5 mm after 4% drift (failure state). However, for the similar drift ratio, the cracking width of the precast specimen was up to 3 times higher than that of the as-built specimen. This indicated that the interface of precast part and post- pouring concrete was relatively weak, which was also previously pointed out by Ref.[42]. Simultaneously, adding extra reinforcement bars and making the rough surfaces provide an alternative way to improve the connecting performance of different parts.

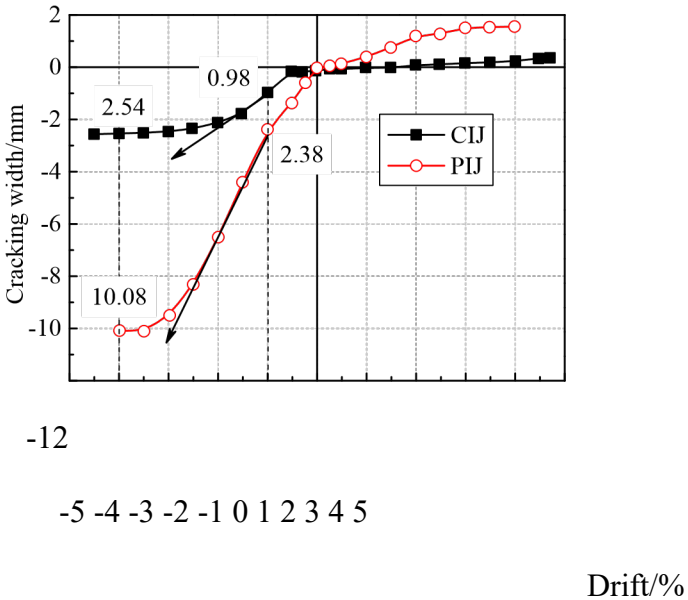

Fig. 20. Cracking width of interfaces for specimens.

5. Study on the thickness of lamination

Based on the aforementioned test results, the hanger bars and rough surface treatment for the laminated slabs recommended by the code were adopted, but the bond strength of interfaces between the precast and cast-in-place elements was still relatively weak, with respect to the cast-in-place concrete slab. Although the bond strength of laminated slab between the precast concrete and the cast-

in-place concrete was excellent and exhibited seismic behavior in the early stage of the test, the obvious bond splitting cracks of the laminated slab were observed in the later stage of loading and directly leads to a significant decrease in the strength of the precast specimen which was also found from the hysteretic curves in Fig. 12. Therefore, the bond strength of the laminated slab was also an important index that affects the mechanical properties of the specimens. In order to reduce this drawback and control the damage of laminated slab, an appropriate lamination thickness ratio, which is obtained by dividing the thickness of precast concrete layer, h_p, with the overall thickness laminated slab, h, is commonly implemented to optimize and evaluate the position of contact interface in the cross-section.

The basic mechanical model which was based on the traditional PSC theory [25,26] was shown in Fig. 21. Many primary assumptions were proposed during the calculation process. 1) the plane section assumption and equivalent rectangular stress diagram were valid; 2) the compression strength of steels may be neglected; 3) the bond strength of the interface between two layers of concrete was good. It was noteworthy that the tensile strength of concrete should be considered, as shown in Fig. 21(b). The interface between two layers of concrete was located in the low stressed zone to reduce the influence of lamination, that was to say, the interface of lamination slab should be as close as to the location of the plastic neutral axis, h_N, in the cross-section, which should enhance indirectly the crack resistance. This measurement was also found in previous studies [25]. The height of the plastic neutral axis was calculated by the force equilibrium method, as shown in Eqs. (3)–(5).

$$N_c = T_s + \alpha_1 f_{ct} b x_t \quad (3)$$

$$x = \frac{\alpha f bh + A^s f^y}{\alpha_1 b(f_{cc} + f_{ct}/\beta)} \quad (4)$$

$$h_N = x_t = \frac{x}{\beta} = h - \quad (5)$$

where, T_s is the longitudinal reinforcement force; f_y is the yielding strength of longitudinal reinforcement; b stands for the width of lamination slab; $\alpha_1$is the concrete stress

intensity factor of 0.85 according to ACI318-14 [43],β is equivalent coefficients which were used to equivalent height, $h_N$represents the height of plastic neutral axis, f_{cc},f_{ct} are the

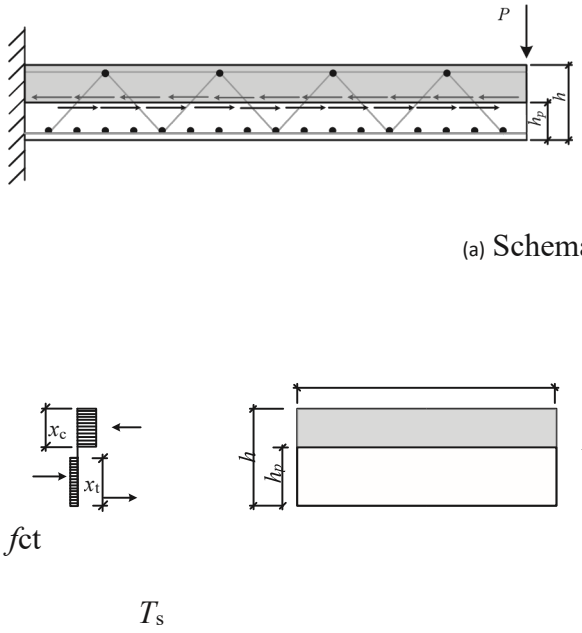

Fig. 21. The mechanical model.

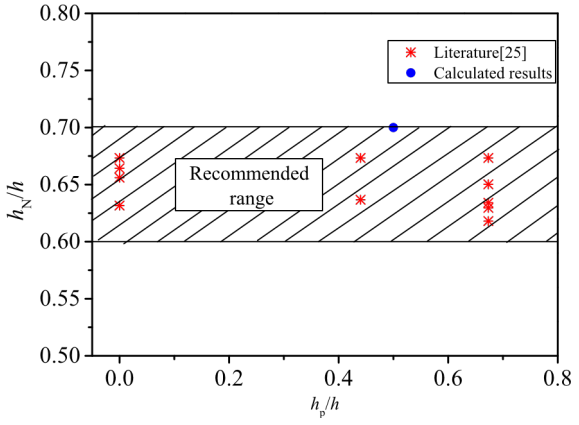

Fig. 22. Recommended range of laminated slab.

compressive and tensile strength, respectively.

Fig. 22 showed the locations of the plastic neutral axis obtained from the literature [25] and this test using the above method. One can see that the thickness ratio of the laminated slab was about 0.6–0.7. That was to say, the thickness ratio of the upper layer (cast-in-place concrete) and lower layer (precast concrete) should be between 3:7 and 2:3. The thickness of precast slab was slightly thicker than that of upper post- pouring slab, which was helpful to improve the construction safety and reduce the on-site construction time due to the precast layer acts as a permanent formwork before casting. Furthermore, the interface between two-layer laminated slabs was located near the plastic neutral axial within the cross-section where the shearing stress was relatively low, which could reduce the influence of the shearing stress as soon as possible, and improve the overall strength of the lamination slabs.

6. Conclusion

The current study presented experimental investigations on two full- scale specimens including a precast beam-slab-column interior joint and a monolithic cast-in-place joint subjected by low-reversed cyclic loading. The seismic behavior of both specimens was studied and compared in terms of failure mode, hysteretic behavior, strength, deformation performance and stiffness degradation. Based on the results of tests, the thickness ratio of the laminated slab was studied. The following conclusions can be drawn:

(1) All specimens underwent similar flexure-dominate failure mode in crushing and spalling at the slab-end concrete. Compared to the cracking distribution of the cast-in-place specimen, failure cracks of the precast specimen always concentrated in the junction between precast elements and post-pouring concrete. In particular, the splitting failure of the laminated slab was exhibited.

(2) The precast joint was capable of matching performance in terms of peaking strength, stiffness, deformation performance of the monolithic connections. It was noteworthy that the precast

specimen exhibited about 60% higher in displacement ductility compared with the corresponding cast-in-place specimen.

(3) A new cross-lapping connection was introduced for bend-up reinforcement at the ends of the semi-precast slab, which can avoid the dense and position contradiction arrangement of the steel in the connection region.

(4) The yielding displacement of cast-in-place specimen was 1.73 times more than that of precast specimens. The elastic–plastic boundary of 1/550 which was utilized to evaluate precast structures should be carefully selected in the design.

(5) An effective range for thickness ratio of upper layer (cast-in-place concrete) and lower layer (precast concrete) varied from 3:7 to

2:3, which could minimize the effects of the interface between two layers on the integrity of lamination slabs.

Declaration of competing interest

The authors declare that they have no known competing financial interests or personal relationships that could have appeared to influence the work reported in this paper.

Acknowledgements

This work was supported by the Beijing Natural Science Foundation (8204054), the National Natural Science Foundation of China (51908013), and the Beijing Postdoctoral International Exchange Funding (2019-PC-10) and the Postdoctoral Foundation of Chaoyang District (2019ZZ-27). Their supports are gratefully acknowledged.

References

[1] Ertas O, Ozden S. Behavior of unbonded, post-tensioned, precast concrete connections with different percentages of mild steel reinforcement. PCI J 2006;52 (2):32–44.

[2] Hawileh R, Rahman A, Tabatabai H. Nonlinear finite element analysis and modeling of a precast hybrid beam–column connection subjected to cyclic loads. Appl Math Model 2010;34(9):2562–83.

[3] Wang HS, Marino EM, Pan P. Design, testing and finite element analysis of an improved precast prestressed beam-to-column joint. Eng Struct 2019;199:109661.

[4] Fan JJ, Wu G, Cao Y. Seismic behaviour of a precast prestressed beam–column joint with energy dissipation bars. Mag Concr Res 2020;72(7):365–78.

[5] Zhang Y, Zhu P, Shi JQ. Flexural behavior of precast UHPC beam with prestressed bolted hybrid joint. Eng Struct 2020;206:110100.

[6] Liu J, Xue YT, Wang CK, Nie JG, Wu ZH. Experimental investigation on seismic performance of mechanical joints with bolted flange plate for precast concrete column. Eng Struct 2020;216:110729.

[7] Jiang HB, Qiu HX, Sun J, Yang Y. Behavior of steel–concrete composite bolted connector in precast reinforced concrete shear wall. Adv Struct Eng 2019;22(12): 2572–82.

[8] Yuksel E, Karadogan HF, Bal IE, Ilki A, Bal A, Inci P. Seismic behavior of two exterior beam–column connections made of normal-strength concrete developed for precast construction. Eng Struct 2015;99:157–72.

[9] Popa V, Papurcu A, Cotofana D, Pascu R. Experimental testing on emulative connections for precast columns using grouted corrugated steel sleeves. Bull Earthq Eng 2015;13(8):2429–47.

[10] Lu ZW, Huang J, Dai SB, Liu JX, Zhang MZ. Experimental study on a precast beam- column joint with double grouted splice sleeves. Eng Struct 2019;199:109589.

[11] Ameli MJ, Parks JE, Brown DN, Pantelides CP. Grouted Splice Sleeve Connection Alternatives for Precast Concrete Bridge Piers in Moderate-to-High Seismic Regions In 2014.

[12] Lu C, Dong BQ, Pan JL, Shan QF, Hanif A, Yin WY. An investigation on the behavior of a new connection for precast structures under reverse cyclic loading.
Eng Struct 2018;169:131–40.

[13] Vidjeapriya R, Jaya KP. Experimental study on two simple mechanical precast beam-column connections under reverse cyclic loading. J Perform Constr Facil
2013;27(4):402–14.

[14] Senturk M, Pul S, Ilki A, Hajirasouliha I. Development of a monolithic-like precast beam-column moment connection: Experimental and analytical investigation. Eng Struct 2020;205:110057.

[15] Stone WC, Cheok GS, Stanton JF. Performance of hybrid moment-resisting precast beam-column concrete connections subjected to cyclic loading. Structural Journal 1995;92(2):229–49.

[16] Liu BK, Zhang YZ, Jin ZF, Shi F, Chang XF. Experimental study on seismic behavior of prestressed fabricated PC frame connections. J Building Structures 2005;26(2):
60–6.

[17] Englekirk R. An innovative design solution for precast prestressed concrete buildings in high seismic zones. PCI J 1996;41(4):44–53.

[18] Zhao B, Lu XL, Liu HF. Experimental study on seismic behavior of precast concrete beam-column subassemblage with cast-in-situ monolithic joint. J Building Structures 2004;25(6):22–8.

[19] Alcocer SM, Carranza R, Perez-Navarrete D, Martinez R. Seismic tests of beam-to- column connections in a precast concrete frame. PCI J 2002;47(3):70–89.

[20] Bull DK, Park R. Seismic resistance of frames incorporating precast prestressed concrete beam shells. PCI J 1986;31(4):54–93.

[21] Liu HT, Xu CS, Du XL. Seismic response analysis of assembled monolithic subway station in the transverse direction. Eng Stuctures 2020;219:110970.

[22] Building Standard Design oCI, Research . JGJ 1-2014,Technical specification for precast concrete structures. China Architecture and Building Press:Beijing. 2014.

[23] Li M, Wang HR, Zhao WJ. Analysis of Mechanical properties of four-sided simple supported two-way laminated slab with shear keys. Advanced Engineering Sciences 2019;51(5):96–106.

[24] Li M, Wang HR, Zhao WJ. Experimental of loading-bearing capacity of one-way laminated slab with shear keys. J Jilin University (Eng Technol Edition) 2020;50 (2):654–67.

[25] Li X, Zheng XY, Ashraf M, Li H. The longitudinal shear bond behavior of an innovative laminated fiber reinforced composite slab. Constr Build Mater 2019; 215:508–22.

[26] Li X, Zheng XY, Ashraf M, Li HT. Experimental study on the longitudinal shear bond behavior of lightweight aggregate concrete–Closed profiled steel sheeting composite slabs. Constr Build Mater 2017;156:599–610.

[27] Hashash YM, Hook JJ, Schmidt B, John I, Yao C. Seismic design and analysis of underground structures. Tunnelling under-ground space Technol 2001;16(4): 247–93.

[28] Imbsen RA. AASHTO guide specifications for LRFD seismic bridge design. A Draft Proposal 2007.

[29] CMC. GB50010-2010,Code for Design of Concrete Structures. Building Industry Press: Beijing, China. 2010.

[30] Wang HS, Barbagallo F, Pan P. Test of precast pre-stressed beam-to-column joint with damage-free reinforced concrete slab. Eng Struct 2020;210:110368.

[31] Liu HT, Du XL. Seismic performance of precast joint in assembled monolithic station: effect of assembled seam shape and position. Earthquakes Structures 2019; 17(6):611–21.

[32] Du XL, Liu HT, Lu DC, Xu CS, Luo FR, Li SM. Study on seismic performance of sidewall joints in assembled monolithic subway station. China Civil Eng J 2017;50 (4):38–47.

[33] Liu HT, Chen JN, Xu CS, Du XL. Seismic performance of precast column connected with grouted sleeve connectors. J Building Eng 2020;101410.

[34] CMC . JGJ/T 101-2015,Specification of seismic test of building. China Architecture and Building Press:Beijing. 2015.

[35] Mashal M, Palermo A. Low-damage seismic design for accelerated bridge construction. J Bridge Eng 2019;24(7):04019066.

[36] ElGawady M, Endeshaw M, McLean D, Sack R. Retrofitting of rectangular columns with deficient lap splices. J Compos Constr 2010;14(1):22–35.

[37] CMC. GB50011-2010 Code for seismic desigh of building. China Architecture and Building Press: Beijing. 2015.

[38] Yang Y, Xue YC, Yu YL, Gao FQ. Experimental study on seismic performance of partially precast steel reinforced concrete columns. Eng Struct 2018;175:63–75.

[39] Gulkan P, Sozen MA. Inelastic responses of reinforced concrete structure to earthquake motions. J. Am. Concr. Inst. 1974;71(12):604–10.

[40] Liu HT, Han Q, Bai YL, Xu CS, Du XL. Connection performance of restrained deformed grouted sleeve splice. Adv Struct Eng 2018;21(3):488–99.

[41] Han W, Zhao Z, Qian J, Cui Y, Liu S. Seismic behavior of precast columns with large-spacing and high-strength longitudinal rebars spliced by epoxy mortar-filled threaded couplers. Eng Struct 2018;176:349–60.

[42] Feng DC, Wu G, Lu Y. Finite element modelling approach for precast reinforced concrete beam-to-column connections under cyclic loading. Eng Struct 2018;174:
49–66.

[43] ACI. Building code requirements for structural concrete (ACI 318–02) and commentary (ACI 318R–02). Am Concrete Institute. In 2002.